

# The nisin–lipid II complex reveals a pyrophosphate cage that provides a blueprint for novel antibiotics

Shang-Te D Hsu<sup>1</sup>, Eefjan Breukink<sup>2</sup>, Eugene Tischenko<sup>1</sup>, Mandy A G Lutters<sup>2</sup>, Ben de Kruijff<sup>2</sup>, Robert Kaptein<sup>1</sup>, Alexandre M J J Bonvin<sup>1</sup> & Nico A J van Nuland<sup>1</sup>

The emerging antibiotics-resistance problem has underlined the urgent need for novel antimicrobial agents. Lantibiotics (lanthionine-containing antibiotics) are promising candidates to alleviate this problem. Nisin, a member of this family, has a unique pore-forming activity against bacteria. It binds to lipid II, the essential precursor of cell wall synthesis. As a result, the membrane permeabilization activity of nisin is increased by three orders of magnitude. Here we report the solution structure of the complex of nisin and lipid II. The structure shows a novel lipid II-binding motif in which the pyrophosphate moiety of lipid II is primarily coordinated by the N-terminal backbone amides of nisin via intermolecular hydrogen bonds. This cage structure provides a rationale for the conservation of the lanthionine rings among several lipid II-binding lantibiotics. The structure of the pyrophosphate cage offers a template for structure-based design of novel antibiotics.

The cell wall is essential for the vitality of bacteria as its strong extracellular peptidoglycan matrix resists the high osmotic pressure of the cytoplasm. It is well conserved throughout evolution and is therefore a prominent target for many antibiotics (reviewed in ref. 1). The monomeric peptidoglycan unit, the basic building block of the cell wall, consists of two amino sugars, *N*-acetylglucosamine (GlcNAc) and *N*-acetylmuramic acid (MurNAc), and a pentapeptide, commonly L-Ala-D-γ-Glu-L-Lys-D-Ala-D-Ala, which is attached to the carboxyl group of MurNAc. These subunits are assembled in the cytosol on a membrane-anchoring carrier, undecaprenyl phosphate, yielding lipid II (GlcNAc-MurNAc-pentapeptide-pyrophosphoryl-undecaprenol, Fig. 1a; reviewed in ref. 2). Lipid II is thereafter transported to the extracellular domain for polymerization of the peptidoglycan moiety.

The essential role of lipid II in cell wall synthesis makes it a target for many antimicrobial peptides<sup>3</sup>. These include vancomycin, the clinical antibiotic of last resort<sup>4</sup>, and ramoplanin, which is now in phase 3 clinical trials<sup>5</sup>. Vancomycin resistance, however, is now emerging<sup>6</sup>. Lipid II is also targeted by nisin, a 34-residue post-translationally modified peptide containing five lanthionine rings and three dehydrated amino acids (Fig. 1b)<sup>7,8</sup>. Lipid II serves not only as an anchoring receptor for nisin but also facilitates the ‘targeted’ pore-forming activity of nisin, thereby reducing the required concentration of nisin for pore formation 1,000-fold<sup>9</sup>. Vancomycin-resistant bacteria with the *vanA*-type gene cluster evade the attack of vancomycin with an epitope substitution of D-Ala-D-Lactate (D-Ala-D-Lac) termini for D-Ala-D-Ala termini in lipid II<sup>6</sup>. In contrast, nisin is still fully active against the *vanA*-type resistant strain, indicating that it binds to lipid II in a different way<sup>9</sup>. The importance of lipid II in cell wall synthesis implies that any

molecule that binds lipid II with high affinity is a potential antibiotic. Therefore, understanding of the recognition mechanism between nisin and lipid II at a molecular level could ultimately lead to the development of novel antibiotics. In this study, we describe the solution structure of nisin–lipid II complex using high-resolution NMR spectroscopy. The structure probably represents the initial step of nisin’s lipid II-mediated pore-formation process. It also illustrates a distinct lipid II-binding mode as compared with that of vancomycin. This recognition mechanism may be generalized to other lipid II-binding lantibiotics, which share the conserved N-terminal lanthionine rings with nisin that form a unique lipid II-binding motif.

## RESULTS

### Solution structure of nisin–lipid II complex

The solution structure of the 1:1 complex of nisin and lipid II was determined in DMSO using a lipid II variant (3LII) with a shortened prenyl tail of 3 isoprene units instead of the 11 in the full-length lipid II (Fig. 1a and Table 1). The lipid tail of lipid II must be of sufficient length to anchor the nisin–lipid II complex in membranes, but replacing the unsaturated isoprene repeats with saturated ones did not impair the pore-forming activity; this suggests that the isoprene repeats are not required for recognition<sup>10</sup>. The short lipid tail of 3LII renders it water-soluble and reduces the number of intense NMR signals originating from the flexible isoprene repeats, leading to poor spectral quality. Although both components separately are water-soluble, the nisin–3LII complex precipitated in aqueous solution. Therefore, we used DMSO to obtain stable and soluble nisin–3LII complex for the NMR studies. DMSO has been used as a membrane

<sup>1</sup>Department of NMR Spectroscopy and <sup>2</sup>Department of Biochemistry of Membranes, Bijvoet Center for Biomolecular Research, Utrecht University, Padualaan 8, 3584CH Utrecht, The Netherlands. Correspondence should be addressed to R.K. (kaptein@nmr.chem.uu.nl) or E.B. (e.j.breukink@chem.uu.nl).

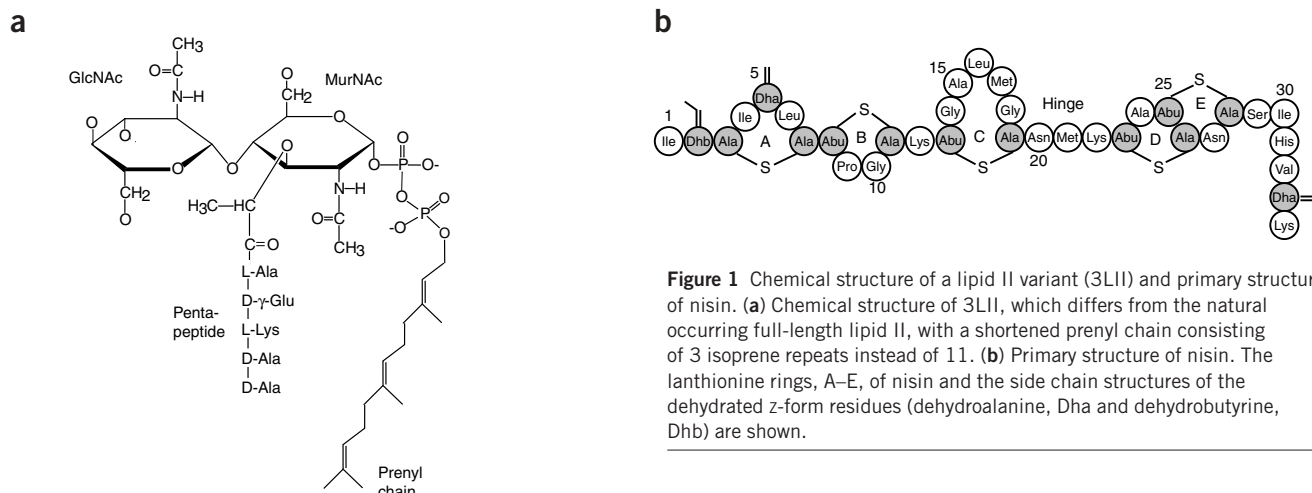


**Figure 1** Chemical structure of a lipid II variant (3LII) and primary structure of nisin. **(a)** Chemical structure of 3LII, which differs from the natural occurring full-length lipid II, with a shortened prenyl chain consisting of 3 isoprene repeats instead of 11. **(b)** Primary structure of nisin. The lanthionine rings, A–E, of nisin and the side chain structures of the dehydrated z-form residues (dehydroalanine, Dha and dehydrobutyryne, Dhb) are shown.

mimetic in several studies, including those of undecaprenyl phosphate, the lipid tail of natural lipid II. NMR spectra of the undecaprenyl phosphate recorded in DMSO have been found to be identical to those obtained in membrane vesicles<sup>11</sup>. Moreover, the dielectric constant,  $\epsilon$ , of DMSO is 47.2 and lies in between that of water ( $\epsilon = 80$ ) and that of the interior of the membrane ( $\epsilon = 2-4$ ), in effect resembling the properties of the interface where the initial nisin-lipid II interaction takes place.

The interface between nisin and 3LII is defined by 36 intermolecular NOEs between residues 1–10 of nisin and MurNAc and the isoprene units of 3LII. In addition, two intermolecular hydrogen bonds were experimentally identified and were used as distance restraints (Table 1).

These involve the amide groups of Dhb2 (dehydrobutyryne) and Abu8 ( $\alpha$ -aminobutyric acid) of nisin and the pyrophosphate moiety of 3LII, as identified by the presence of the cross hydrogen bond nitrogen-phosphorous ( $^{15}\text{N}-\text{H}\cdots\text{O}-^{31}\text{P}$ ) scalar coupling  $^3J_{\text{NP}}$  (see Methods and Fig. 2). The nisin–3LII complex is well defined at the interface with a rather disordered tail (Fig. 3a and Table 1). This is supported by the fact that a reduction of the intrinsic flexibility of nisin upon 3LII binding is only observed in the N-terminal part, as indicated by the heteronuclear  $^{15}\text{N}\{^1\text{H}\}$ -NOE data (Fig. 3b). The formation of intermolecular hydrogen bonds and close contacts with the highly electronegative phosphate moiety induces large chemical shift perturbations in the N-terminal part of nisin, in line with those previously observed in the lipid II-containing SDS micelles<sup>12</sup> (Fig. 2 and Supplementary Fig. 1 online). Owing to the large number of modified residues (Fig. 1b), nisin exhibits no canonical secondary structure, but does contain type I  $\beta$ -turns in rings B and C and two consecutive type II and II'  $\beta$ -turns in the intertwined rings D and E. In contrast to the extended and flexible structure in the absence of 3LII (data not shown), upon binding to 3LII, the N terminus of nisin folds back onto the first two lanthionine rings, A and B, forming a cage-like structure. This cage encompasses the pyrophosphate group of 3LII with a buried surface area of  $842 \pm 86 \text{ \AA}^2$ . This represents more than a third of the 3LII total solvent-accessible surface. Except the side chains of Ala3 and Ala7, which are part of the lanthionine ring linkage, all other side chains reside at the rim of

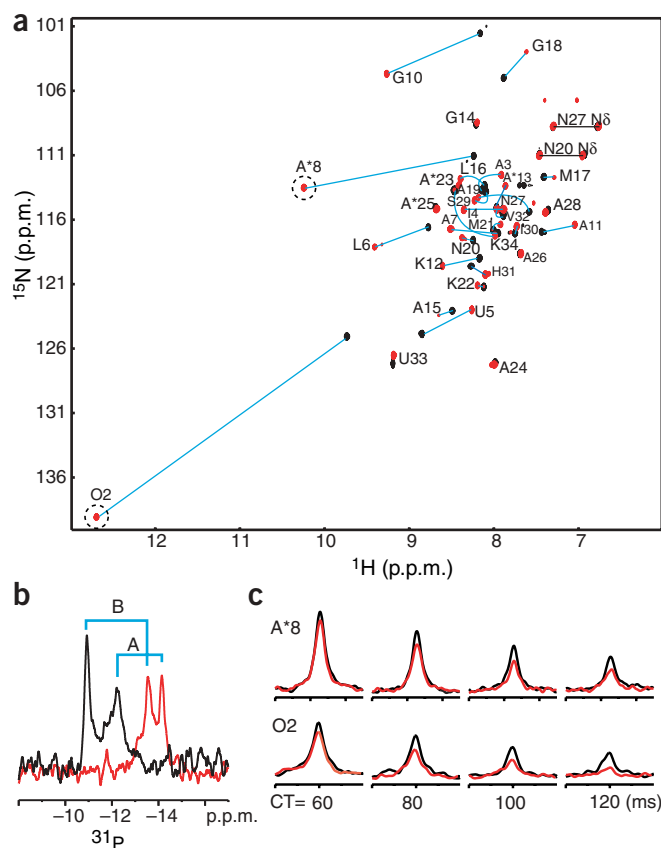


**Figure 2** Formation of nisin–3LII complex. **(a)** Overlaid  $^1\text{H}-^{15}\text{N}$  HSQC spectra of the free (black) and 3LII-bound (red) nisin. Changes in chemical shifts are indicated by cyan lines with corresponding residue labels (U, dehydroalanine; O, dehydrobutyryne; A\*,  $\alpha$ -aminobutyric acid). The amide protons of O2 and A\*8 that are hydrogen-bonded to the pyrophosphate group of 3LII are indicated by dashed circles. The hydrogen bond formation is responsible for the large downfield shifts along the proton dimension. **(b)**  $^{31}\text{P}$  NMR spectra of the pyrophosphate group of 3LII in the free (black) and nisin-bound (red) forms ( $\Delta\delta P_A = -1.91$  p.p.m. and  $\Delta\delta P_B = -2.62$  p.p.m.). Signals A and B correspond to the individual phosphates that are attached to the MurNAc moiety and the prenyl chain, respectively (Fig. 1a). The upfield shifts of the two phosphorous nuclei are a result of intermolecular hydrogen bond formation. **(c)** Cross-sections of the O2 and A\*8 signals along the  $^1\text{H}$  dimension in the  $^{31}\text{P}$ -edited constant time (CT)  $^1\text{H}-^{15}\text{N}$  HSQC<sup>22,23</sup>. The intensities of these hydrogen-bonded amides are modulated by the cross hydrogen bond scalar coupling to the phosphorous ( $^3J_{\text{NP}}$ ) and are attenuated owing to transverse relaxation decay during the CT delays (red). The reference experiment with  $^{31}\text{P}$  decoupling during CT delays removes the  $^3J_{\text{NP}}$  coupling modulation (black).

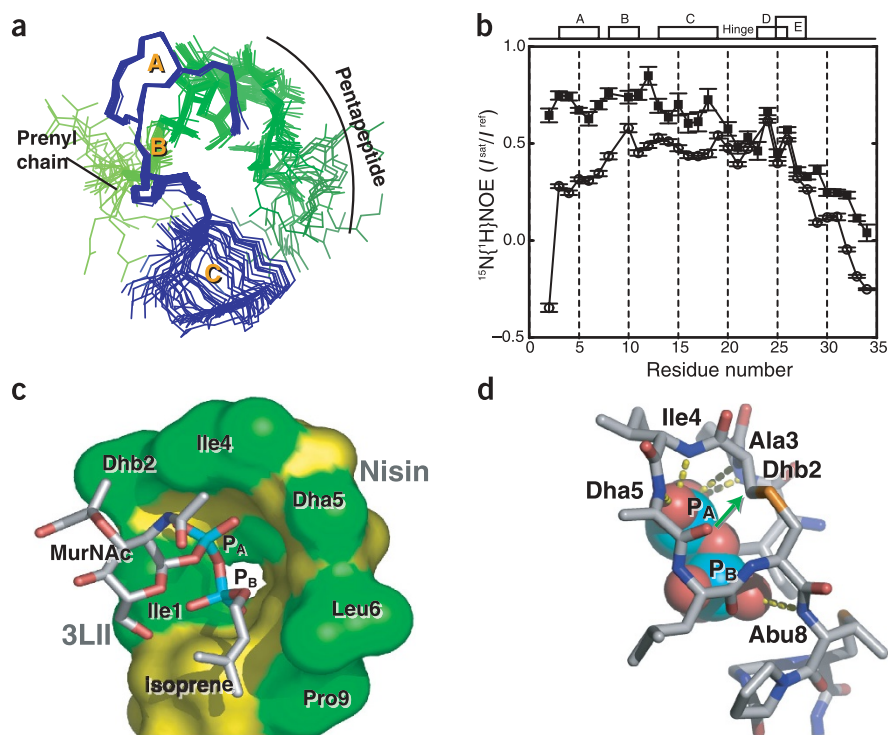


**Figure 3** Solution structure of nisin–3LII complex. **(a)** Ensemble of the 20 lowest-energy NMR structures superimposed on the heavy atoms of the interface of the complex (see Table 1). The backbone of nisin (residues 1–19), including lanthionine linkages, is blue with the lanthionine rings A–C labeled (see Fig. 1b). The unstructured C-terminal part is omitted for clarity. The pentapeptide, MurNAc, GlcNAc, pyrophosphate moiety and the prenyl chain of 3LII are colored from dark to light green. **(b)**  $^{15}\text{N}\{^1\text{H}\}$  heteronuclear NOEs of nisin in the free (○) and complex (■) forms.  $^{15}\text{N}\{^1\text{H}\}$  NOE is given by the ratio of the  $^1\text{H}$ -saturated (on-resonance) and reference (off-resonance) peak intensities ( $I^{\text{sat}}/I^{\text{ref}}$ ). An amide group in a structured region will have a value close to 1 whereas an amide group in an unstructured, flexible region will have a value close to 0, or even below. **(c)** The N-terminal part of nisin (residues 1–12 shown in van der Waals surface with backbone and side chain atoms in yellow and green, respectively) encages the pyrophosphate moiety of 3LII. The side chains (green) of nisin are labeled. Carbon, nitrogen, oxygen and phosphorus atoms of 3LII are white, blue, red and cyan, respectively. **(d)** Nisin backbone–3LII pyrophosphate intermolecular hydrogen bond network. Hydrogen bonds with high occurrence in the ensemble of structures, defined by LIGPLOT<sup>28</sup>, are indicated by yellow dashed lines and the corresponding residues are labeled (pyrophosphate group in spheres). The sulfur atoms in the lanthionine rings are orange. A green arrow indicates the position of Ala3-C $\beta$ , at which addition of a methyl group can disrupt the bioactivity (see text for details). The figures were generated using PyMOL (<http://www.pymol.org/>).

the binding cleft (Fig. 3c). The unique backbone architecture of the pyrophosphate cage allows the formation of five intermolecular hydrogen bonds between the backbone amides of nisin and the pyrophosphate group (Fig. 3d). By contrast, another polyprenylpyrophosphate-binding molecule, the mammalian farnesyltransferase, coordinates the pyrophosphate group solely via hydrogen bonding with conserved side chains<sup>13</sup>. As preorganization with lanthionine linkages provides a lower entropy loss upon binding, this may well be the dominant factor in the recognition mechanism of the pyrophosphate group of lipid II.

### The pyrophosphate cage is a novel lipid II-binding motif

The binding mode involving the pyrophosphate moiety revealed here shows that nisin does not target the same motif of lipid II as does vancomycin<sup>9</sup>, and possibly ramoplanin<sup>5</sup>. It also explains why nisin does not differentiate between lipid II and lipid I, which differ in the GlcNAc moiety<sup>3</sup>. The chemical shift changes in D-Ala-D-Ala and the terminal

isoprene units of 3LII upon nisin binding are negligible (Supplementary Fig. 1 online); only a localized perturbation was observed in the  $\beta$ 1–4 linkage between MurNAc and GlcNAc. These leave the pyrophosphate, MurNAc and the first isoprene in lipid II and the N-terminal part of nisin as the determinants for nisin–lipid II recognition. The structure of the complex explains several earlier observations. First, extension of the N terminus, as in ITPQ-nisin, which contains four additional residues (I, T, P and Q) at the N terminus, markedly diminishes the antimicrobial activity<sup>14</sup>. Second, the introduction of an extra methyl group at the side chain of Ala3, S3T-nisin, decreases the lipid II binding affinity of nisin 50-fold (ref. 15). In contrast, similar modifications in the second position, Dhb2, had little effect<sup>15</sup>. Third,  $\Delta$ Ala5-nisin, with ring A nicked open by hydrolytic cleavage, is biologically inactive<sup>16</sup>. All these observations can be rationalized by examining the interface of the complex: (i) because the side chain of the N-terminal Ile1 is part of the interface (Fig. 3c), extension of the N terminus may interfere with the interfacial complementarity; (ii) the additional methyl group in S3T-nisin sterically hampers the formation of intermolecular hydrogen bonds (see green arrow in Fig. 3d); (iii) the rigidity of the ring structure is lost owing to ring opening and hence the intermolecular hydrogen bond between Dha5 and the pyrophosphate moiety is destabilized.

### DISCUSSION

Throughout evolution, the lanthionine ring structure of nisin, in particular rings A and B, is well conserved among several lipid II-binding lantibiotics<sup>7,8</sup>. Efforts to create more effective antibiotics by changing the side chain compositions of nisin-like peptides have achieved only a marginal improvement of bioactivity so far<sup>17</sup>. This can now be understood, because binding to lipid II is dictated

mainly by the backbone scaffold of the ring structures. Using the nisin–3LII complex as a template, we carried out homology modeling of several related lantibiotics containing conserved lanthionine rings A and B (Fig. 4a). This revealed that the pyrophosphate cage can accommodate a variety of side chain compositions. Apart from the conserved positions 3 and 7–11, all observed differences among the homologs reside at the circumference of the pyrophosphate cage. The occurrence of various amino acid types, both hydrophilic and hydrophobic, suggests that the side chain interactions are of minor importance in lipid II binding. Notably, the hydrophobic character at position 6 remains preserved. This residue interacts with the prenyl chain and possibly also with the membrane bilayer in which lipid II is anchored. The notion of a common motif for lipid II recognition is supported by the observation that lipid II is also the target of other lantibiotics such as epidermin<sup>3</sup> and mutacin 1140 (E.B., unpublished data) (Fig. 4b). We therefore propose that the pyrophosphate cage is the general lipid II-binding architecture for these lantibiotics.

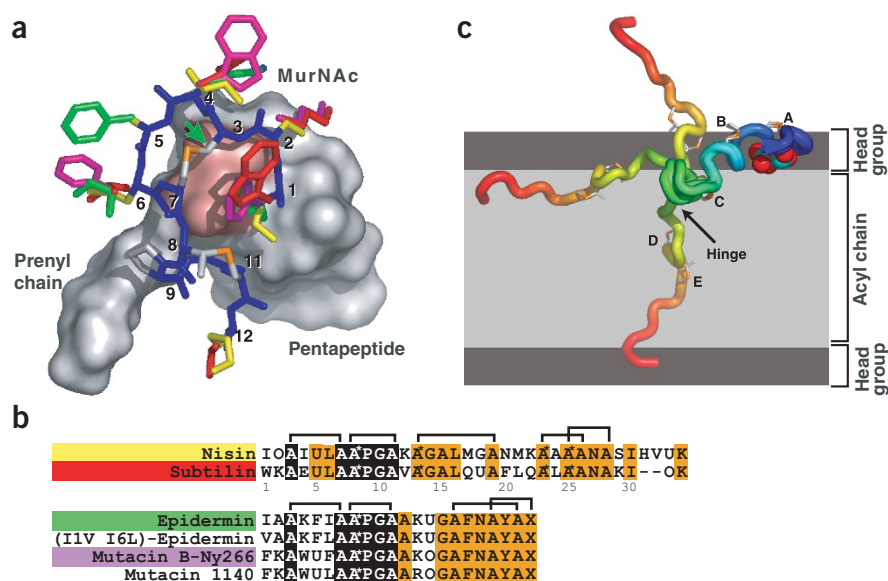


**Figure 4** Structure-based homology modeling and model of pore formation. **(a)** General binding model of lipid II-binding lantibiotics. *In silico* mutagenesis was carried out to model the side chains (see below) of subtilin (red), epidermin (green) and mutacin B-Ny266 (purple) based on the nisin structure (yellow). The backbone is blue with the conserved side chains in white and the sulfur atoms of the lanthionine rings in orange. Only the first 12 residues are shown; 3LII is shown in van der Waals surface with the pyrophosphate moiety in pink. The position of the Ala3 side chain is indicated by a green arrow. The structure has the same orientation as in **Figure 2a**. **(b)** Primary sequence alignment of type A lantibiotics. Nisin and subtilin form a subfamily of type A lantibiotics. Another subfamily consists of epidermin (I1V I6L)-epidermin, mutacin B-Ny266 and mutacin 1140 (refs. 8,29) with a cyclized C terminus (X, 2-aminovinyl-D-cysteine, AviCys). The universally conserved residues are highlighted in black and the conserved residues within the subfamilies are highlighted in orange. The lanthionine linkages are indicated above each subfamily. **(c)** Model of the nisin-lipid II complex in a membrane bilayer. The backbone of three representative structures of nisin are shown and colored from blue to red from N to C termini. Each conformation, taken from the ensemble of structures of the nisin-3LII complex, corresponds to a possible orientation of the C-terminal part of nisin outside, on the surface, or inserted into the membrane bilayer, respectively. They are positioned so that the pyrophosphate group of 3LII (spheres) is at the same depth as head groups of lipid molecules (dark gray) in a membrane with a thickness of ~40 Å, which is based on a molecular dynamics simulation of free lipid II in explicit membrane bilayer (S.-T.D.H. and A.M.J.J.B., unpublished data).

The formation of a 1:1 nisin-lipid II complex is the first step toward pore formation. Once nisin is anchored onto lipid II on the membrane surface, subsequent conformational changes take place that lead to the assembly of a higher-order oligomeric complex<sup>10</sup>. Pore formation requires a transmembrane orientation of nisin involving insertion of its C-terminal part<sup>18</sup> and a flexible hinge region (residues 20–22)<sup>15</sup>. One could conjecture the early stage of this multistep process on the basis of the present structure of the nisin-3LII complex. The positioning of the N-terminal part of nisin with respect to the prenyl chain may already pave the way for subsequent membrane insertion. Assuming that the interface of the nisin-3LII complex is preserved in the membrane bilayer, we propose a model for the membrane insertion of nisin based on the current nisin-3LII complex (**Fig. 4c**). This shows that initially ring C of nisin would readily be embedded into the membrane at a depth comparable to that of the first few isoprene repeats (**Fig. 4c**). The modeling demonstrates that nisin can span the membrane bilayer with the pyrophosphate cage as the anchoring point. However, this requires conformational flexibility in the hinge region, which is depicted by three conformations taken from the ensemble of calculated structures (**Fig. 4c**). Lack of a flexible hinge by truncation or proline replacement would hamper this insertion process, explaining the lack of pore-formation activity of these mutants<sup>15</sup>.

In conclusion, this study has revealed a novel lipid II recognition motif for nisin and related lantibiotics. The pyrophosphate moiety plays an essential role in the synthesis of the bacterial cell wall. Its chemical entity is the Achilles' heel of bacteria that cannot be altered or replaced by simple mutations as opposed to alteration of the attached pentapeptide that can lead to vancomycin resistance. Since its discovery in 1928, nisin has been used as a food preservative and in animal health products, such as treatments for mastitis. On the other hand, penicillin, which was discovered at the same time as nisin, is no longer effective for the treatment of hospital-acquired infections, as reported by the World Health Organization (WHO, <http://www.who.int/>). In essence, the structure of the nisin-3LII complex described here can provide a basis for future antibiotic design.

## METHODS

**Sample preparation.** Uniformly <sup>15</sup>N-labeled nisin and unlabeled 3LII were produced as described<sup>10,12</sup>. The nisin-3LII complex was prepared by mixing equal molar amounts of lyophilized [*U*-<sup>15</sup>N]nisin and 3LII in water followed by centrifugation. The supernatant was removed and the insoluble complex pellet was rinsed with water several times. The pellet was lyophilized and dissolved in 99.9% perdeuterated d<sub>6</sub>-DMSO (Cambridge Stable Isotope) to reach a final concentration of ~1.2 mM. Free [*U*-<sup>15</sup>N]nisin and 3LII samples were prepared by dissolving the lyophilized sample into d<sub>6</sub>-DMSO to reach similar sample concentrations.

**NMR spectroscopy.** NMR spectra were recorded at 300 K on Bruker DRX500, DRX600, DRX750 and DRX900 spectrometers equipped with a triple-resonance or a cryogenic probe (DRX600) for <sup>1</sup>H, <sup>15</sup>N and <sup>13</sup>C detection and a multinuclear (DRX500) or a broadband probe (DRX600) for <sup>31</sup>P detection. Spectra were processed with NMRPipe<sup>19</sup> and analyzed using NMRView<sup>20</sup>. The <sup>1</sup>H and <sup>15</sup>N chemical shifts were assigned using standard methods<sup>21</sup>. <sup>13</sup>C chemical shifts of the well-resolved peaks were assigned from <sup>1</sup>H-<sup>13</sup>C heteronuclear single quantum correlation spectroscopy (HSQC) and <sup>1</sup>H-<sup>13</sup>C heteronuclear multiple bond correlation spectroscopy (HMBC)<sup>21</sup> recorded with natural abundance. The two <sup>31</sup>P chemical shifts of the pyrophosphate groups in 3LII were distinguished by <sup>1</sup>H-<sup>31</sup>P HMBC. The cross hydrogen bond scalar coupling <sup>3</sup>J<sub>NP</sub> was identified by <sup>31</sup>P-edited constant time (CT) <sup>1</sup>H-<sup>15</sup>N HSQC<sup>22,23</sup> with and without <sup>31</sup>P decoupling during the constant time delays of 60, 80, 100 and 120 ms. The assigned chemical shift data sets were deposited in the BioMagResBank under accession codes 6144, 6145 and 6146 for free nisin, free 3LII and their complex, respectively.

**Structure calculation and modeling.** Distance restraints were derived from two-dimensional homonuclear <sup>1</sup>H-<sup>1</sup>H NOESY and three-dimensional <sup>15</sup>N NOESY-HSQC. Intermolecular restraints were obtained from <sup>15</sup>N-edited filter experiments<sup>21</sup>. Two experimentally identified intermolecular hydrogen bonds (Dhb2-NH and Abu8-NH to pyrophosphate group in 3LII) were introduced in the later stages of the calculations as ambiguous distance restraints from the amide groups to any of the oxygen atoms in the pyrophosphate group with bounds of 1.6–2.4 Å (H-O) and 2.5–3.3 Å (N-O). Backbone ϕ dihedral angle restraints were derived from <sup>3</sup>J<sub>HN,Hα</sub> coupling constants determined by three-dimensional HNHA<sup>21</sup>. The side chain rotameric states (χ1) were derived from

**Table 1** NMR and refinement statistics for the nisin–3LII complex

	Nisin	3LII
<b>NMR distance and dihedral constraints</b>		
Distance restraints		
Total NOE	509	110
Intra-residue	241	66
Inter-residue		
Sequential ( $ i - j  = 1$ )	175	37
Non-sequential ( $ i - j  > 1$ ) <sup>a</sup>	83	7
Nisin–3LII intermolecular	36	
Intermolecular hydrogen bonds <sup>b</sup>	4	
Total dihedral angle restraints		
Nisin	13	0
Backbone $\phi$	6	0
Side chain $\chi_1$	7	0
<b>Structure statistics<sup>c</sup></b>		
Violations (mean and s.d.)		
Distance constraints (Å)	0.049 ± 0.003	
Dihedral angle constraints (°)	0.40 ± 0.19	
Max. distance constraint violation (Å)	0.42	
Deviations from idealized geometry		
Bond lengths (Å)	0.00060 ± 0.00002	
Bond angles (°)	1.63 ± 0.03	
Improper (°)	1.01 ± 0.04	
Average pairwise r.m.s. deviation among refined structures (Å)		
Nisin		
Heavy (residues 1–12)	0.49 ± 0.16	
Backbone (residues 1–12)	0.25 ± 0.09	
Heavy (all)	6.93 ± 2.35	
Backbone (all)	6.23 ± 2.30	
3LII		
All heavy	2.67 ± 0.73	
Complex		
Interface heavy <sup>d</sup>	0.56 ± 0.16	

<sup>a</sup>3LII has a branched structure where the pentapeptide, GlcNAc and polyprenyl pyrophosphate are branched from MurNAc (Fig. 1a). Therefore the nonsequential distance restraints of 3LII are defined as those that are not present between two adjacent amino acids, sugars or prenyl units. <sup>b</sup>Each experimentally determined intermolecular hydrogen bond is defined by two distance restraints (for details, see Results and Methods). <sup>c</sup>The statistics were obtained from an ensemble of 20 lowest-energy solution structures of the largest cluster of the nisin–3LII complex. The structures were refined in a shell of explicit DMSO solvent model<sup>27</sup>. <sup>d</sup>The interface of the complex is defined as residues 1–12 of nisin and MurNAc, pyrophosphate moiety and the first isoprene unit of 3LII (110 heavy atoms).

the intensity-based comparison of NOESY and double quantum filter-correlation spectroscopy (DQF-COSY) spectra<sup>24</sup>. The experimentally determined distance and dihedral restraints (Table 1) were applied in a simulated annealing protocol using CNS<sup>25</sup> and HADDOCK<sup>26</sup> with nisin and 3LII treated as fully flexible for docking. The structures were refined using an explicit DMSO solvent model<sup>27</sup>. Owing to the large amount of modified D- and Z-form (Dha and Dhb) amino acids (Fig. 1b), conventional Ramachandran plot analysis is not a suitable measure of structural quality. Of the regular L-form amino acids, only Asn20 and Met21, which lie in the intrinsically flexible hinge region, had  $\phi$  and  $\psi$  angles in the disallowed region of the Ramachandran plot (2 and 15 out of 20 structures, respectively). Homology modeling was done using PyMOL (<http://www.pymol.org/>) from the representative structure of the nisin–3LII complex (the closest to the mean). Side chains were mutated *in silico* followed by manual adjustment of the rotamer conformations and subsequent energy minimization.

**Coordinates.** The atomic coordinates of the nisin–3LII complex have been deposited in the Protein Data Bank (accession code 1UZT).

*Note: Supplementary information is available on the Nature Structural & Molecular Biology website.*

## ACKNOWLEDGMENTS

This work was in part supported through the National NMR facility at Utrecht University from the Netherlands Organization for Chemical Research (NWO-CW). A.M.J.J.B. is a recipient of a NWO Jonge Chemici grant. A.M.G.L. is supported by NWO-STW grant 349-5257. We thank E.J. Smid (NIZO-food research) for his help with the preparation of <sup>15</sup>N-labeled nisin.

## COMPETING INTERESTS STATEMENT

The authors declare that they have no competing financial interests.

Received 5 May; accepted 16 July 2004

Published online at <http://www.nature.com/nsmb/>

- Koch, A.L. Bacterial wall as target for attack: Past, present, and future research. *Clin. Microbiol. Rev.* **16**, 673–687 (2003).
- van Heijenoort, J. Biosynthesis of the bacterial peptidoglycan unit. In *Bacterial Cell Wall* Vol. 27 (eds. Ghuysen, J.-M. & Hakenbeek, R.) 39–54 (Elsevier Science B.V., Amsterdam, 1994).
- Brötz, H. *et al.* Role of lipid-bound peptidoglycan precursors in the formation of pores by nisin, epidermin and other lantibiotics. *Mol. Microbiol.* **30**, 317–327 (1998).
- Sheldrick, G.M., Jones, P.G., Kennard, O., Williams, D.H. & Smith, G.A. Structure of Vancomycin and its complex with acetyl-D-alanyl-D-alanine. *Nature* **271**, 223–225 (1978).
- McCafferty, D.G. *et al.* Chemistry and biology of the Ramoplanin family of peptide antibiotics. *Biopolymers* **66**, 261–284 (2002).
- Hughes, D. Exploiting genomics, genetics and chemistry to combat antibiotic resistance. *Nat. Rev. Genet.* **4**, 432–441 (2003).
- Sahl, H.-G. & Bierbaum, G. LANTIBIOTICS: Biosynthesis and biological activities of uniquely modified peptides from Gram-positive bacteria. *Annu. Rev. Microbiol.* **52**, 41–79 (1998).
- Guder, A., Wiedemann, I. & Sahl, H.-G. Posttranslationally modified bacteriocins—the lantibiotics. *Biopolymers* **55**, 62–73 (2000).
- Breukink, E. *et al.* Use of the cell wall precursor lipid II by a pore-forming peptide antibiotic. *Science* **286**, 2361–2364 (1999).
- Breukink, E. *et al.* Lipid II is an intrinsic component of the pore induced by nisin in bacterial membranes. *J. Biol. Chem.* **26**, 26 (2003).
- Zhou, G.P. & Troy, F.A. 2nd. Characterization by NMR and molecular modeling of the binding of polyisoprenols and polyisoprenyl recognition sequence peptides: 3D structure of the complexes reveals sites of specific interactions. *Glycobiology* **13**, 51–71 (2003).
- Hsu, S.-T. *et al.* Mapping the targeted membrane pore formation mechanism by solution NMR: The nisin Z and lipid II interaction in SDS micelles. *Biochemistry* **41**, 7670–7676 (2002).
- Long, S.B., Casey, P.J. & Beese, L.S. Reaction path of protein farnesyltransferase at atomic resolution. *Nature* **419**, 645–650 (2002).
- Kuipers, O.P., Rollema, H.S., de Vos, W.M. & Siezen, R.J. Biosynthesis and secretion of a precursor of nisin Z by *Lactococcus lactis*, directed by the leader peptide of the homologous lantibiotic subtilin from *Bacillus subtilis*. *FEBS Lett.* **330**, 23–27 (1993).
- Wiedemann, I. *et al.* Specific binding of nisin to the peptidoglycan precursor lipid II combines pore formation and inhibition of cell wall biosynthesis for potent antibiotic activity. *J. Biol. Chem.* **276**, 1772–1779 (2001).
- Chan, W.C., Bycroft, B.W., Lian, L.Y. & Roberts, G.C.K. Isolation and characterisation of two degradation products derived from the peptide antibiotics nisin. *FEBS Lett.* **252**, 29–36 (1989).
- Liu, W. & Hansen, J.N. Enhancement of the chemical and antimicrobial properties of subtilin by site-directed mutagenesis. *J. Biol. Chem.* **267**, 25078–25085 (1992).
- van Heusden, H., de Kruijff, B. & Breukink, E. Lipid II induces an overall transmembrane orientation of the pore-forming peptide lantibiotic nisin. *Biochemistry* **41**, 12171–12178 (2002).
- Delaglio, F. *et al.* NMRPipe: a multidimensional spectral processing system based on UNIX pipes. *J. Biomol. NMR* **6**, 277–293 (1995).
- Johnson, B.A. & Blevins, R.A. NMRView: a computer program for the visualization and analysis of NMR data. *J. Biomol. NMR* **4**, 603–614 (1994).
- Cavanagh, J., Fairbrother, W.J., Palmer III, A.G. & Skelton, N.J. *Protein NMR Spectroscopy* (Academic Press, San Diego, CA, 1996).
- Mishima, M. *et al.* Intermolecular <sup>31</sup>P–<sup>15</sup>N and <sup>31</sup>P–<sup>1</sup>H scalar couplings across hydrogen bonds formed between a protein and a nucleotide. *J. Am. Chem. Soc.* **122**, 5883–5884 (2000).
- Löhr, F., Mayhew, S.G. & Rüterjans, H. Detection of scalar couplings across NH...OP and OH...OP hydrogen bonds in a flavoprotein. *J. Am. Chem. Soc.* **122**, 9289–9295 (2000).
- Basus, V.J. Proton nuclear-magnetic-resonance assignments. *Methods Enzymol.* **177**, 132–149 (1989).
- Brünger, A.T. *et al.* Crystallography & NMR system: a new software suite for macromolecular structure determination. *Acta Crystallogr. D* **54**, 905–921 (1998).
- Dominguez, C., Boelens, R. & Bonvin, A.M.J.J. HADDOCK: a protein-protein docking approach based on biochemical or biophysical information. *J. Am. Chem. Soc.* **125**, 1731–1737 (2003).
- Linge, J., Williams, M.A., Spronk, C.A.E.M., Bonvin, A.M.J.J. & Nilges, M. Refinement of protein structures in explicit solvent. *Proteins* **50**, 496–506 (2002).
- Wallace, A.C., Laskowski, R.A. & Thornton, J.M. LIGPLOT: a program to generate schematic diagrams of protein ligand interactions. *Protein Eng.* **8**, 127–134 (1995).
- Smith, L. *et al.* Covalent structure of mutacin 1140 and a novel method for the rapid identification of lantibiotics. *Eur. J. Biochem.* **267**, 6810–6816 (2000).